coatings

MDPI

Article

Enhanced Anti-Tribocorrosion Performance of Ti-DLC Coatings Deposited by Filtered Cathodic Vacuum Arc with the Optimization of Bias Voltage

Yongqing Shen [1], Jun Luo [1,*], Bin Liao [2], Lin Chen [1], Xu Zhang [2], Yuanyuan Zhao [1], Pan Pang [1] and Xinmiao Zeng [1,*]

[1] Institute of Radiation Technology, Beijing Academy of Science and Technology, Beijing 100875, China; shenyq0529@163.com (Y.S.); lchen1209@163.com (L.C.); zhaoyuanyuanchn@163.com (Y.Z.); pyxiskid@163.com (P.P.)

[2] Key Laboratory of Beam Technology of Ministry of Education, College of Nuclear Science and Technology, Beijing Normal University, Beijing 100875, China; liaobingz@bnu.edu.cn (B.L.); zhangxu@bnu.edu.cn (X.Z.)

* Correspondence: luojun@brc.ac.cn (J.L.); sherry_0282_cn@sina.com (X.Z.)

Abstract: To improve the anti-tribocorrosion property, and decrease the metal dissolution and wear of stainless-steel components caused by the synergistic action of corrosion and friction in marine environments, Ti-DLC coatings were obtained on steel substrate using a filtered cathodic vacuum arc (FCVA) system by adjusting bias voltage. The structure, mechanical properties, corrosion, and tribocorrosion behavior were investigated. Increasing the bias voltage from −50 V to −300 V, Ti content decreased from 23.9 to 22.5 at.%, and grain size decreased first, and then increased. Obvious TiC grains embedded in the amorphous carbon matrix were observed in the coating from the TEM result. Hardness increased from 30.23 GPa to 34.24 GPa with an increase in bias voltage from −50 to −200 V. The results of tribocorrosion testing showed that the Ti-DLC coatings at −200 V presented the best anti-tribocorrosion performance with the smallest friction coefficient of 0.052, wear rate of 2.48×10^{-7} $mm^3/N{\cdot}m$, and high open-circuit potential, which is mainly due to the dense structure, high value of H/E^* and H^3/E^{*2}, and great corrosion resistance. Obtained results suggest that the Ti-DLC coating with nanocomposite structure is a potential protective material for marine equipment.

Keywords: Ti-DLC coatings; filtered cathodic vacuum arc; tribocorrosion

Citation: Shen, Y.; Luo, J.; Liao, B.; Chen, L.; Zhang, X.; Zhao, Y.; Pang, P.; Zeng, X. Enhanced Anti-Tribocorrosion Performance of Ti-DLC Coatings Deposited by Filtered Cathodic Vacuum Arc with the Optimization of Bias Voltage. *Coatings* **2022**, *12*, 697. https://doi.org/10.3390/coatings12050697

Academic Editor: Christian Mitterer

Received: 26 April 2022
Accepted: 17 May 2022
Published: 19 May 2022

1. Introduction

Marine tribocorrosion has become one of the most important and difficult problems to be solved for the safety and economic use of marine equipment such as ships and thrust bearings in harsh seawater environments. Stainless steel has been widely used in structural components in marine fields. However, stainless steel would degrade or fail under the synergy between corrosion and wear in seawater environments [1–3]. Thus, it is of great significance to develop a protective coating with great tribocorrosion performance. The tribocorrosion behavior is the interaction between corrosion and wear, which would lead to more serious damage than pure wear or corrosion [4], Thus, tribocorrosion experiments of coatings and steel are needed to further study the tribocorrosion mechanism and decrease wear of stainless-steel components.

In recent years, different coatings have been reported in literature for anti-tribocorrosion coatings, such as TiN, CrSiN, and VCN [4–6]. Liu et al. [7] found that VCN showed lower i_{corr} and coefficient of friction than VN coating due to the incorporation of C. Diamond-like carbon (DLC) films with high hardness, chemical inertness, low wear rate, and high corrosion resistance, which have attracted much attention as candidates for protective material to enhance wear and corrosion behavior [8,9]. Doping elements can decrease residual stress and improve properties of DLC coatings, such as N, Si elements, which can enhance

thermal stability, and Cu, which could improve corrosion resistance [10–12]. Among them, the incorporation of Ti could release residual stress, and improve adhesion and mechanical properties, which could further improve DLC comprehensive property [13]. In addition, Ti doping in DLC coating could lead to the formation of nanocomposite structure, where TiC nanoclusters are embedded in an amorphous carbon matrix. It was found that the unique structure of nanocomposite coatings could provide a large number of interfaces and small grain size, which prevent the initiation and propagation of cracks [14,15]. Therefore, Ti doping in DLC coating is expected to further enhance comprehensive performance. Many studies [13–15] have reported the effect of Ti content on the microstructure, mechanical, and tribological properties of Ti-DLC coatings. It is well known that ion energy has huge influence on the growth of coatings, which leads to the different structure and properties of the coatings [16–18]. Zhang [16] found that the microstructure of NbC coatings was closely related to negative bias, and high ion energy could enhance the diffusion of adsorbed atoms. Dai [19] studied the effect of bias voltage on Cr-DLC film, and the results showed that negative bias would lead to different chromium concentration of the films and carbide phase, which results in different mechanical properties. Khamseh et al. [20] showed that internal stress, hardness, and plasticity index of the a-C: Nb coating increased with an increase in bias voltage. Microstructure and corrosion protection characteristics evolution were also investigated. Therefore, the structure, mechanical, and anti-corrosion properties of the coatings could be optimized through adjusting negative bias voltage. However, surprisingly, few works have investigated the effect of bias voltage on the structure, friction, and corrosion properties of Ti-DLC films, and the tribocorrosion performance of films in seawater environment is still rare and remains unknown.

The filtered cathodic vacuum arc (FCVA) is an effective method to deposit nanocomposite films, because it can control the deposition energy more accurately and with high plasma density. This method has become one of the most promising techniques [21]. In a previous study, the effect of Ti content on microstructure and tribocorrosion behavior of Ti-DLC films was investigated [15]. In this work, the Ti-DLC were deposited on stainless steel and Si substrate at different negative bias voltages. The effect of bias voltage on microstructure, mechanical property, corrosion, and tribocorrosion behavior of Ti-DLC films in a seawater environment were studied, and then the evolution of friction and corrosion behavior in seawater was explored. This study aims to obtain protective Ti-DLC films with outstanding comprehensive properties for marine mechanical parts in seawater conditions.

2. Experimental Methods

2.1. Coating Preparation

Ti-DLC coatings were deposited on AISI 304L stainless steel (20 mm × 20 mm × 3 mm) and (100) Si substrates by filtered cathodic vacuum arc technology under C_2H_2 reactive gas flows. The schematic of the FCVA equipment is given elsewhere [22]. Before the experiment, the substrates were ultrasonically cleaned in ethanol and acetone (15 min), and dried by clean nitrogen. The samples were assembled on a rotated holder. The Ti target with a purity of 99.99 was used as a cathode. The arc current was 100 A and positive bias was 24 V. During the deposition, the C_2H_2 flow was kept constant of 80 sccm. A series of coatings were deposited by adjusting the bias voltages from −50 to −300 V. The deposition time of all coatings was the same (20 min) to ensure a similar thickness.

2.2. Coating Characterization

The bonding states were examined using X-ray photoelectron spectroscopy (XPS, VG ESCALABMKII, South Manchester, UK), and the coatings were etched with Ar^+ for 30 s to remove contaminant on the surface before measurement. The atomic composition was estimated by area of each peak such as C 1 s in XPS spectra. The crystallographic structure of coatings was evaluated using X-ray diffraction (XRD, Xpert Pro MPD, Almelo, The Netherlands). The grain size was calculated based on Scherrer's formula. The surface roughness and three-dimensional surface morphology of the coatings were assessed using

an atomic force microscope (AFM; Tosca™ 400, Graz, Austria). The cross-sectional morphology and elemental composition were examined by scanning electron microscopy (SEM, Hitachi S-4800, Tokyo, Japan) equipped with an energy-disperse spectroscopy system (EDS, EMAX-350, Tokyo, Japan). The microstructure was evaluated by transmission electron microscopy (HRTEM, Jem-2100, Hillsboro, USA), and the coatings were prepared on a single-crystalline NaCl substrate. The thickness of the as-deposited coatings was examined by a surface morphology instrument (Talysurf 5P-120, Leicester, UK). The adhesion was evaluated by a Rockwell indenter (HRA, Lanzhou, China). The hardness and Young's modulus were obtained using the nano-indenter (MML Nano Test P3, Wales, UK) with a diamond Berkovich indenter tip. The indentation depth was limited to 100 nm, which is around 8% of the coating thickness, to eliminate the influence of steel substrate. For each sample, six indentations were measured.

2.3. Tribocorrosion Experiments

The tribocorrosion test device (MFTR4000, Lanzhou, China) was a linear reciprocating mode integrated with a three-electrode cell configuration. A Si_3N_4 ball with a diameter of 6 mm was used as counterpart. During the test, constant normal load was 2 N, the length of wear tracks was 5 mm, and frequency was set at 1 Hz. All the tribocorrosion tests were tested in 3.5 wt% NaCl aqueous solution. Three samples prepared at one condition were tested separately in the same experiment conditions to avoid accidental error, and all tests were carried out at room temperature. The following two kinds of tests were assessed to evaluate the tribocorrosion performance of the substrate and the coatings in 3.5 wt% NaCl solution.

(1) Open-circuit potential (OCP). Before testing, the samples were immersed in 3.5 wt% NaCl solution for approximately 1 h to reach a stable potential. The evolution of potential and coefficient of friction (COF) were recorded. The morphology and cross-section profiles of the wear scars of the coating after tribocorrosion testing were measured by SEM and surface morphology, respectively. The wear rates were calculated based on the equation: $\omega = V/F \times S$, where V, F, S represent wear volume, applied load, and sliding distance, respectively.

(2) The potentiodynamic polarization test, which was conducted by conventional three-electrode glass cell in the 3.5 wt% NaCl aqueous solution. The samples, platinum wire, and saturated calomel (SCE) were used as the working electrode, auxiliary electrode, and reference electrode, respectively. The scanning rate was 1 mV/s.

3. Results and Discussion

3.1. Characteristics of Ti-DLC Coating

The chemical composition and deposition parameters are given in Table 1, and were obtained by XPS. With the increase in negative bias voltage from −100 to −300 V, the thickness of the coating sees a little decrease, which is mainly caused by the effect of ion bombardment. In addition, the Ti content decreases from 23.9 to 22.5 at.%, while the carbon content increases from 69.3 to 71.3 at.% as the bias voltage increases from −50 to −300 V. With the increase in bias voltage, enhanced collision, bombardment, and resputtering may lead to an increase in the carbon content due to the relatively lower sputtering yield of the carbon atoms. The content of amorphous carbon monotonously increases with increasing bias voltage.

The cross-section morphology of the deposited Ti-DLC coatings at varied bias voltages is shown in Figure 1. As seen, the columnar microstructure of the coating is less pronounced, with all coatings showing columnar-free and dense structure, especially the coating deposited at −200 V. A Ti transition layer with thickness of 100 nm was prepared to enhance the adhesion between the Ti-DLC coating and steel substrate. Figure 2 shows the TEM image of the coating prepared at −200 V and the corresponding SAED pattern. It can be seen from the TEM image that the coating shows typical nanocomposite structure and TiC grains are embedded in the amorphous a-C matrix. The selected area electron

diffraction (SAED) image shows three diffraction rings, which correspond to TiC (1 1 1), TiC (2 0 0), and TiC (2 2 0) from inside to outside, respectively. The electron diffraction rings of the coating are weak, which corresponds to a high amount of amorphous carbon.

Table 1. The chemical composition, thickness, and deposition parameters of Ti-DLC coating.

Sample	Bias Voltage (V)	Composition (at.%)			Thickness (μm)	Amorphous Carbon Content (%)
		Ti	C	O		
1	−50	23.9	69.3	6.8	1.12	52.5
2	−100	23.6	70.2	6.2	1.15	53.8
3	−200	23.2	70.8	6.0	1.08	54.3
4	−300	22.5	71.3	6.2	1.07	55.3

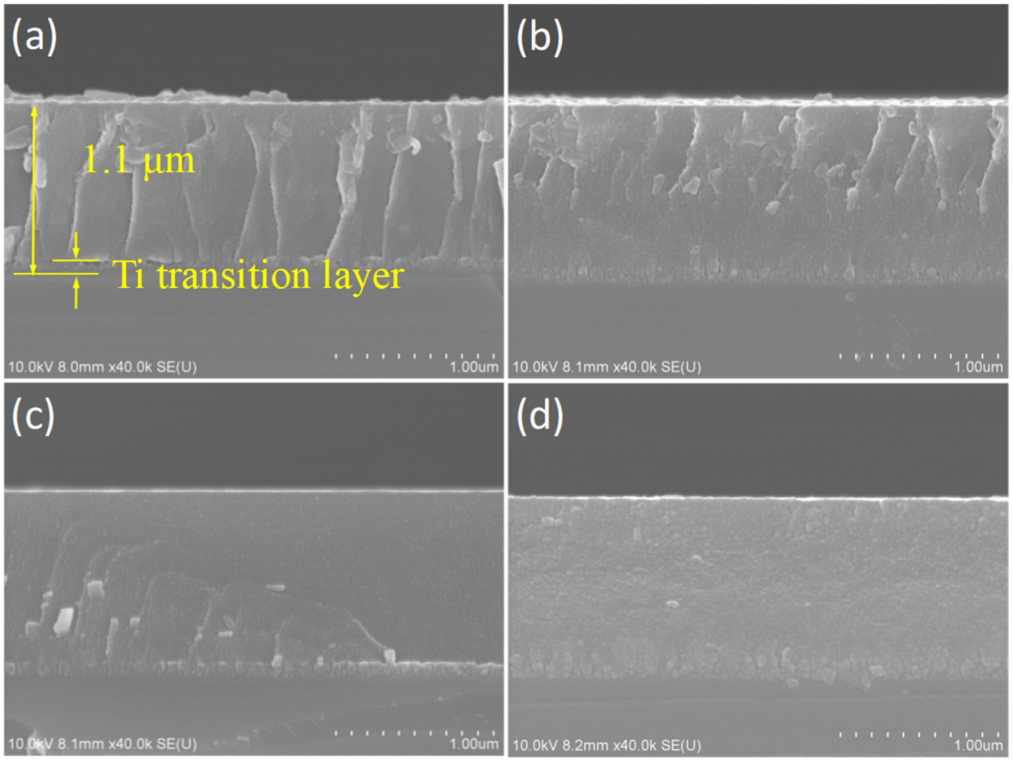

Figure 1. SEM images of cross-sections of Ti-DLC coatings prepared at varied substrate bias: (**a**) −50 V, (**b**) −100 V, (**c**) −200 V, and (**d**) −300 V.

The RMS roughness (Rq) was obtained from AFM topography. Figure 3 shows the three-dimensional images of the Ti-DLC coatings. The results show that the Rq values of Ti-DLC coatings prepared at varied bias voltage ranges from 1 to 3 nm, manifesting that the Ti-DLC coatings are dense and smooth. At −50 V, the coating shows an obvious granular structure. Increasing the voltage from −50 V to −100 V, the values of Rq of Ti-DLC coatings decrease from 2.44 nm to 1.05 nm. With the increase in bias voltage, the morphology of the coatings surface changes to shallow dome, leading to the decrease in surface roughness. Peng [23] found that the preferential formation of graphitic clusters at low ion energy may lead to granular morphology. With increasing the bias voltage, increased ion energy promotes surface diffusion, ion bombardment, and sputter, which results in the smoother surface. However, high bias voltage also results in the heating of the substrate, which would cause roughness of the coating. In this work, a change in bias voltage from −100 to −300 V has a subtle influence on the roughness of the coatings.

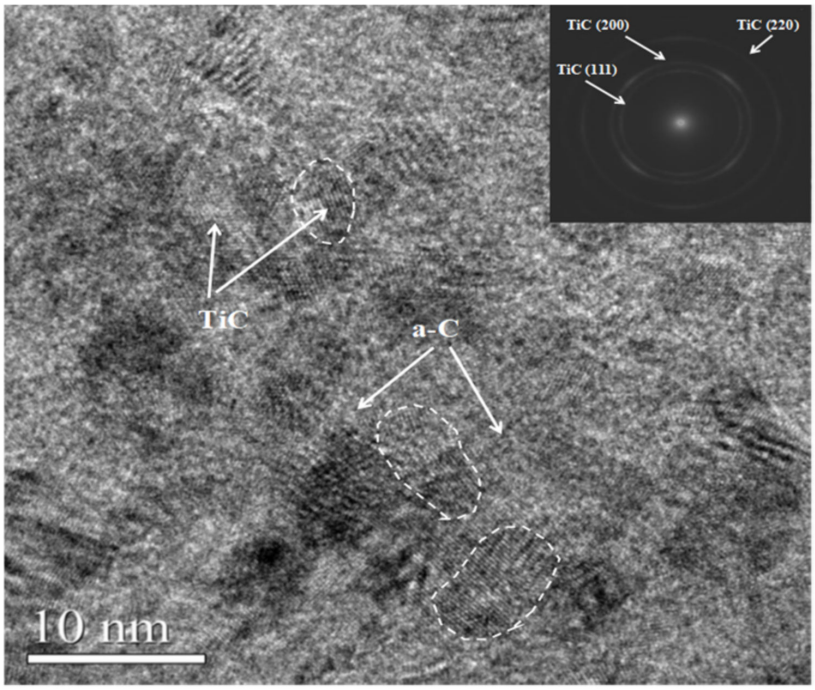

Figure 2. TEM image and SAED pattern of the coating at −200 V.

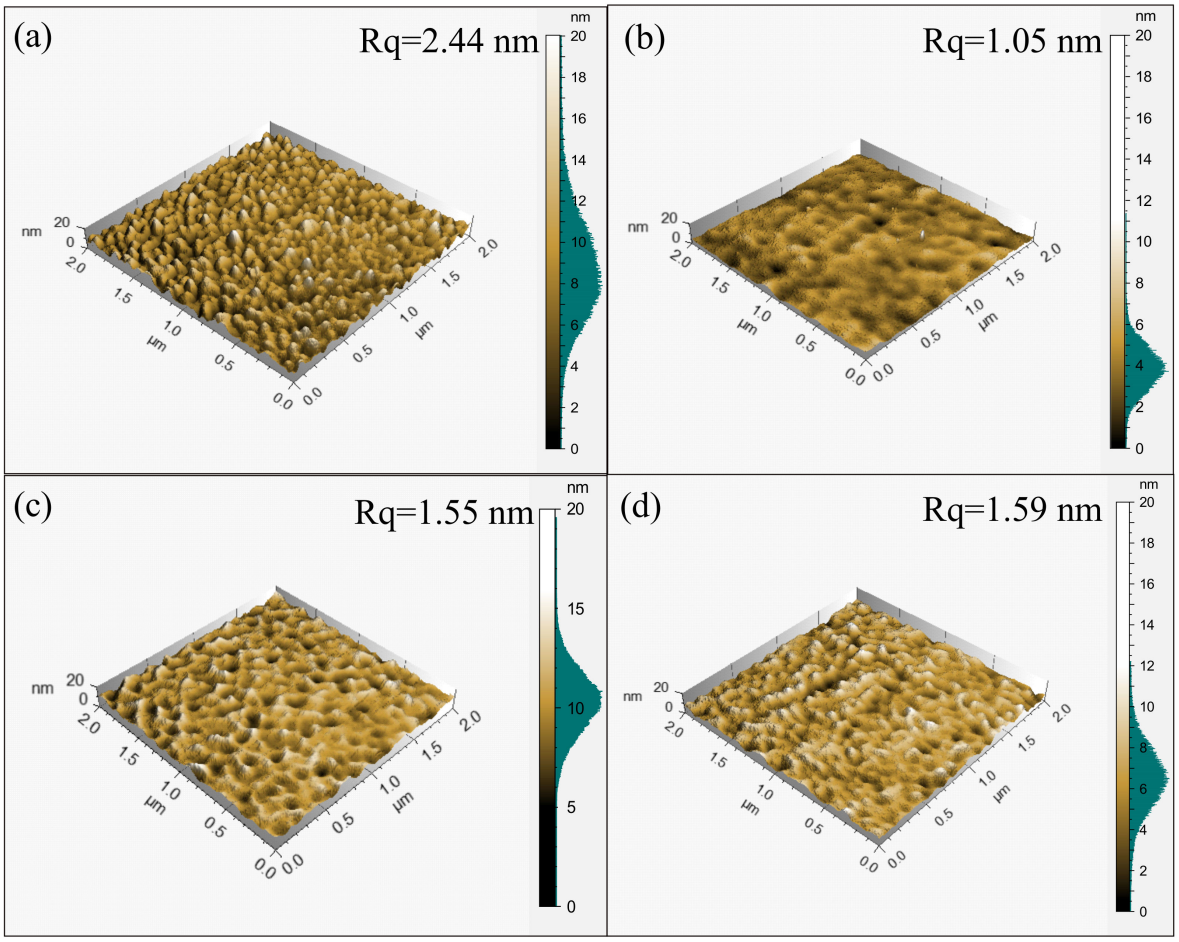

Figure 3. AFM micrographs and the RMS roughness (Rq) of the Ti-DLC coatings prepared at different substrate bias voltages: (**a**) −50 V, (**b**) −100 V, (**c**) −200 V, and (**d**) −300 V.

The XRD pattern of Ti-DLC coatings prepared at varied bias voltages are given in Figure 4a. The diffraction peaks (1 1 1), (2 0 0), and (2 2 0) of TiC (ICSD 89-3828) at 35.8°, 41.6°, and 60.4°are observed. The peaks of (2 0 0) and (2 2 0) are less obvious. As seen in Figure 4a, the intensity of the TiC (1 1 1) peak increases first and then decreases. The preferential orientation of (111) is related to the surface energy [24]. The variation in intensity and width of diffraction peaks can reflect the crystallinity and grain size of the coatings. The grain size of the Ti-DLC coatings prepared under varied bias voltage calculated from TiC (1 1 1) peak is presented in Figure 4b. With the increase in substrate bias, the grain size of coating at −200 V is smallest, however, the grain size of the Ti-DLC coatings is almost consistent, which is around 5.4 nm. The increased ion beam energy with increase in negative bias would promote nucleation and reduce grain size. The grain size is also related to the temperature of the substrate. The high ion energy could lead to an increase in substrate temperature and the diffusion length of surface-migrating atoms facilitates the atomic migration and grain growth [25]. Consequently, the grain size decreases first and then increases with increasing bias voltage.

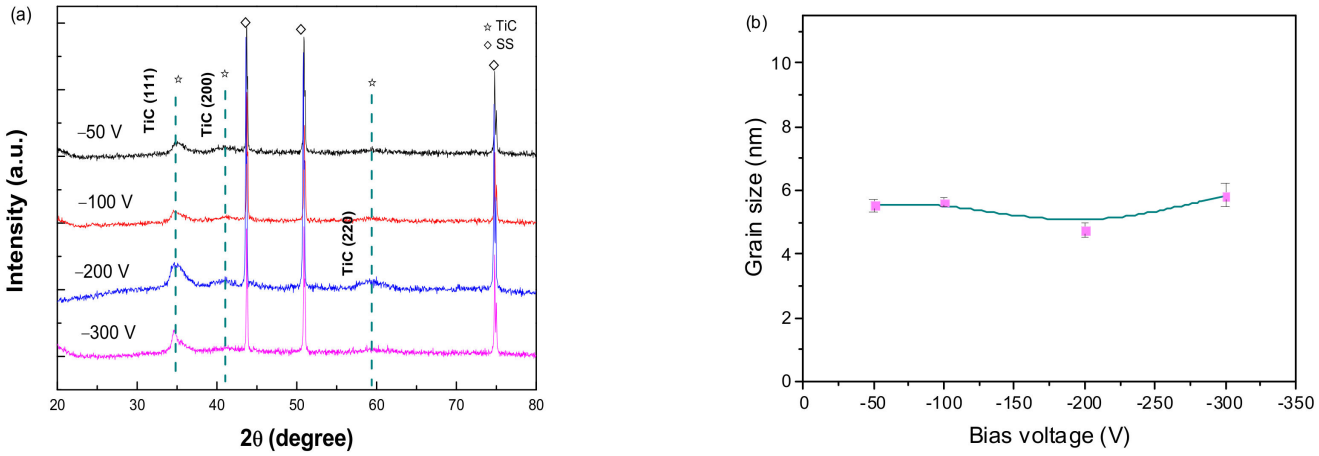

Figure 4. XRD pattern (**a**) and average grain size (**b**) of as-prepared Ti-DLC coatings.

Due to the high chemical sensitivity, XPS analysis was used to detect the bonding state of titanium in the coating. The C 1s and Ti 2p spectra of Ti-DLC coatings deposited at different bias voltages are given in Figure 5. As seen, there are two obvious peaks located at 281.8 eV and 284.6 eV of the C1s spectrum, which correspond to C in TiC and a-C:H, respectively. C 1s spectra is deconvoluted into five peaks at 281.8, 282.6, 284.6, 285.6, and 288.6 eV, which are assigned to Ti-C, Ti-C*, sp^2C, sp^3C, and C=O, respectively, and the Ti-C* represent the non-stoichiometric TiC_x [26,27]. The Ti 2p XPS spectra can be fitted into four peaks: the peaks at 453.6 eV and 459.3 eV are assigned to Ti-C bonds, the peak at 454.7 eV is identified as non-stoichiometric TiC_x, and the peak located at 456.8 eV is assigned to Ti-O/T=O bond [28,29]. The intensity of Ti-C bond increases in the C 1s spectra of coating with an increase in bias voltage from −50 to −200 V, consistent with the increase in the intensity of TiC peak (1 1 1) obtained in the XRD result.

3.2. Mechanical Properties

Hardness (H) and Young's modulus (E) of the Ti-DLC coatings prepared at different bias voltages are shown in Figure 6a. As displayed, the H (E) increases from 30.23 GPa (279.23 GPa) to 34.24 GPa (304.92 GPa) with an increase in bias voltage from −50 V to −200 V. Increasing bias voltage to −300 V, the H and E present the lowest values of 29.11 GPa and 262.8 GPa, respectively. The ratios of H/E* (E*, effective Young's modulus) and H^3/E^{*2} are related to the elastic strain to failure and the plastic deformation resistance of the coatings [30,31]. The results of H/E* and H^3/E^{*2} of all prepared coatings are given in Figure 6b. As seen, although H/E* and H^3/E^{*2} first increase and

then decrease with increasing bias voltage, which shows the same trend with the results of H and E, the coatings at −100 V exhibit the highest values of H/E* and H^3/E^{*2} of 0.12 and 0.45, respectively. Thus, the coating prepared at −100 V has the best durability and plastic deformation resistance among all coatings [32]. The high hardness of the coating mainly due to the hardness enhancement mechanism of the nanocomposite coating. The strong interface between nanocrystalline and amorphous phases can effectively prevent dislocation migration and crack propagation, which can improve the H and E of the coating [33]. Some researchers attribute increased hardness of Ti-DLC coating with increasing bias voltage to increased coating density during the growth of the coating [34]. In addition, according to the mechanism of hardness enhancement, the hardness of the Ti-DLC coatings is related to the content of TiC, grain size, and the integrity and thickness of the amorphous carbon [35,36]. According to the results of XRD, the coating at −200 V shows small TiC grain size. From the results obtained above, the dense structure, small grain size, and the fine content of TiC phase may be mainly accountable for the high hardness, H/E*, and H^3/E^{*2} of coating at −100 V and −200 V.

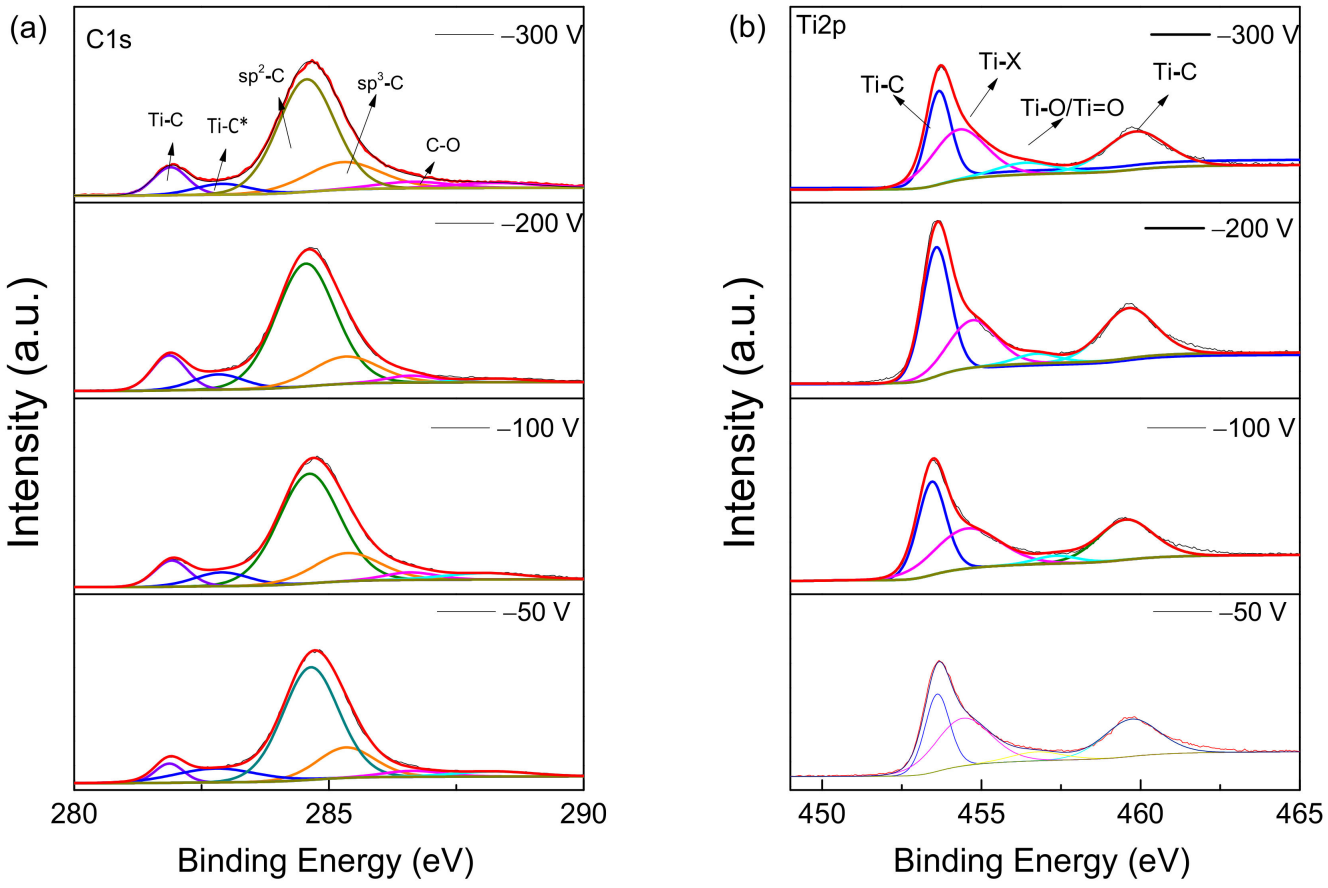

Figure 5. The C 1s (**a**) and Ti 2p (**b**) spectra of Ti-DLC coatings at varied bias voltage.

The adhesion strength test of Ti-DLC coatings was carried out using a Rockwell indenter HR-150. The SEM micrograph indentation morphologies of Ti-DLC coatings deposited under different bias voltages after Rockwell tests are demonstrated in Figure 7. All coatings show great adhesion of above HF1, and no radial cracks or delamination appear at the indentation boundary. The excellent adhesion strength between the substrate and coating can be ascribed to presence of the transition Ti interlayer.

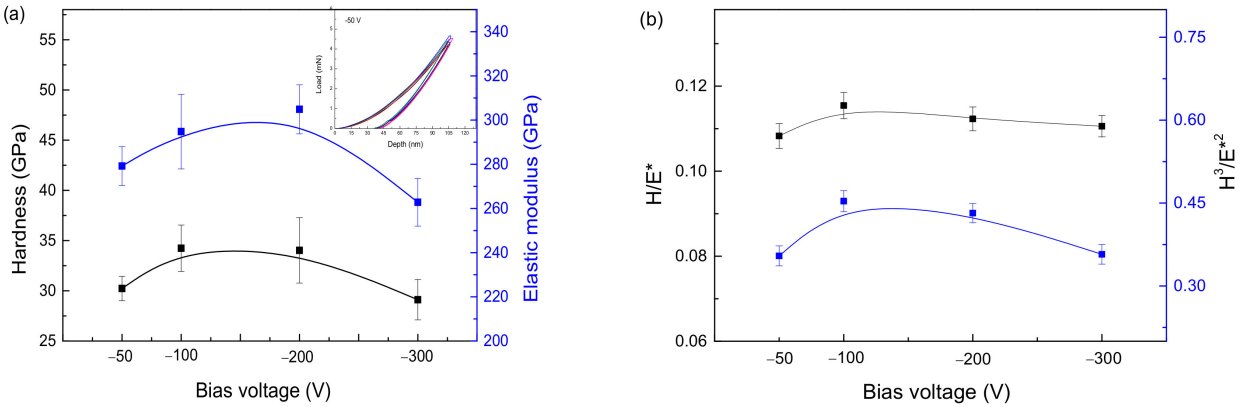

Figure 6. Hardness, Young's modulus (**a**), and H/E* and H^3/E^{*2} (**b**) of Ti-DLC coatings deposited under different bias voltages, the load–displacement curves of Ti-DLC coatings at −50 V on the top-right corner of (**a**).

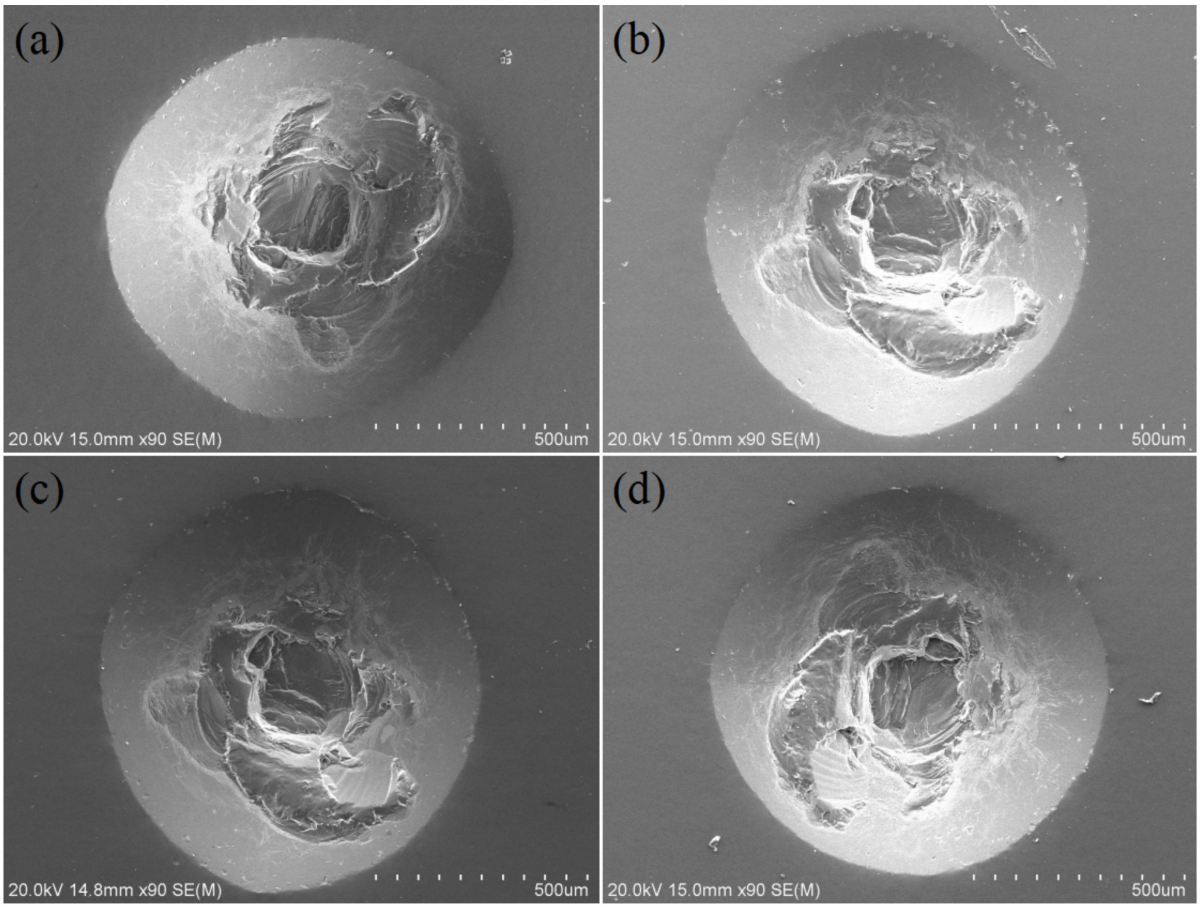

Figure 7. SEM micrograph indentation morphologies of Ti-DLC coatings at different bias voltages after Rockwell C tests: (**a**) −50 V; (**b**) −100 V; (**c**) −200 V, and (**d**) −300 V.

3.3. Tribocorrosion Performance

The potentiodynamic polarization curves of Ti-DLC coatings prepared at different bias voltages in 3.5 wt% NaCl aqueous solution under static and sliding condition are demonstrated in Figure 8. The fitting results, such as corrosion current density (I_{corr}), corrosion potential (E_{corr}), and polarization resistance (R_p) in the corrosion state and sliding state are listed in Table 2.

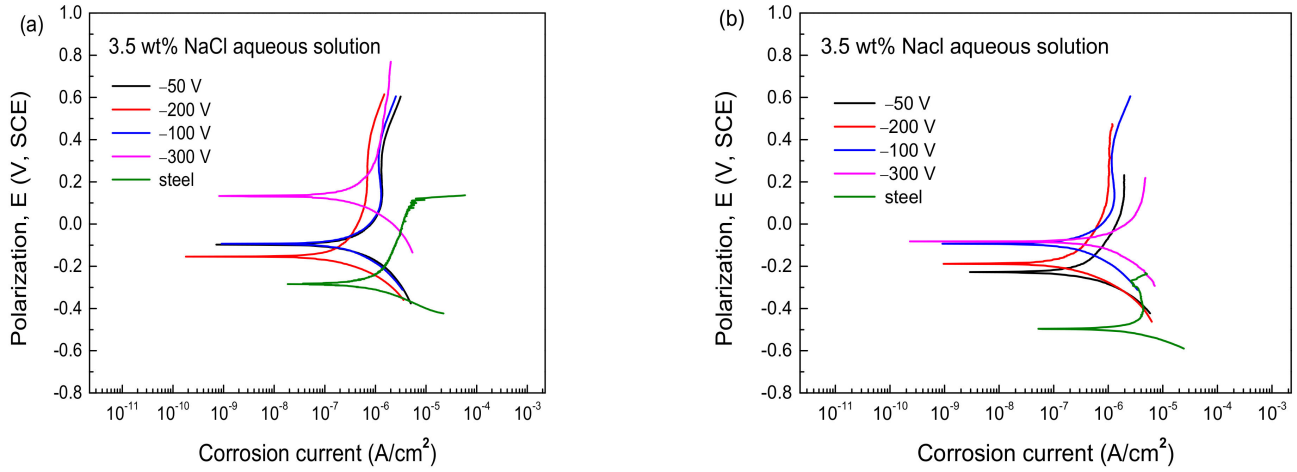

Figure 8. Potentiodynamic polarization curves of Ti-DLC coatings under: (**a**) corrosion-only (**b**) sliding in 3.5 wt% NaCl aqueous solution.

Table 2. The fitting results of the polarization curves in the corrosion state and sliding state.

Specimens	Corrosion-Only			Sliding			Porosity
	I_{corr} ($\times 10^{-7}$ A/cm^2)	E_{corr} (V)	R_p ($\times 10^8$ Ω·cm^2)	I_{corr} ($\times 10^{-7}$ A/cm^2)	E_{corr} (V)	R_p ($\times 10^8$ Ω·cm^2)	
Steel	13.75	−0.29	0.47	20.52	−0.50	0.21	/
−50	2.85	−0.10	4.12	3.21	−0.23	2.55	9.1
−100	2.72	−0.10	4.85	2.81	−0.22	3.51	6.1
−200	1.97	−0.17	5.21	2.12	−0.19	3.98	6.5
−300	3.28	0.12	3.02	8.08	−0.09	2.64	8.1

The polarization resistance (R_p) of the coating was calculated by the following formula [37]:

$$R_p = \frac{\beta_a \times \beta_c}{2.303 \times I_{corr}(\beta_a + \beta_c)} \quad (1)$$

where the β_a and β_c are the anode and cathode Tafel slopes and I_{corr} represents the corrosion current density. Porosity is one of the most significant parameters to evaluate the corrosion resistance of the materials. The porosity (P/%) can be estimated by empirical formula [38]:

$$P = \left(R_{pm(substrate)} / R_{p(coating-substrate)}\right) \times 10^{-|\Delta E_{corr}/\beta_a|} \quad (2)$$

where R_{pm} is the polarization resistance of the substrate. ΔE_{corr} represents the difference in corrosion potential between coating and bare substrate.

During the corrosion process, an obvious passivation feature is observed on the curve, suggesting the formation of passivation coating. In the corrosion-only process, compared with the Ti-DLC coatings, the steel substrate shows the highest I_{corr} value and the lowest R_p value, indicating the better anti-corrosion performance of Ti-DLC coatings compared to substrate [39,40]. For the Ti-DLC coating, with increasing bias voltage from −50 to −200 V, the value of I_{corr} decreases from 2.85 × 10^{-7} A/cm^2 to 1.97 × 10^{-7} A/cm^2 and the R_p value increases from 4.12 × 10^8 Ω·cm^2 to 5.21 × 10^8 Ω·cm^2. Compared with the reported VN, CrN, etc., the value of I_{corr} Ti-DLC is lower, suggesting good corrosion resistance of Ti-DLC coatings in artificial seawater [4–6]. With continued increase in bias voltage, the R_p value decreases. Compared with the corrosion process, the E_{corr} and R_p of all coatings and substrate decrease in the tribo-corrosion process. It is worth noting that I_{corr} and E_{corr} of the coatings at −200 V only show little change from 1.97 × 10^{-7} A/cm^2 to 2.12 × 10^{-7} A/cm^2 and −0.17 V to −0.19 V, respectively, and the change is less pronounced. Meanwhile, the I_{corr} value of the coating at −300 V is greatly decreased during the sliding process,

indicating that the friction process can exacerbate corrosion. The increase in I_{corr} and drop in E_{corr} of coating and substrate during the sliding conditions are attributed mainly to the damage or removal of the passivation coating on the corrosion surface caused by mechanical wear. In addition, Ti-DLC coating at −200 V shows the lowest I_{corr} and the highest R_p both in the static and sliding process, indicating the best corrosion resistance of the coating. According to Manhabosco et al. [41], porosity has an important influence on the electrochemical properties of the coating, and even a low index porosity can promote the diffusion of corrosion solution through the coating, which may penetrate into coating and leads to the delamination of the coating in local corrosion. The porosity of the coatings is calculated and given in Table 2. The coatings at −100 V and −200 V have low porosity at about 0.06, which is mainly due to the dense structure of the coating. This also could explain the good anti-corrosion property of the coating at −200 V. The coating at −50 V shows the highest porosity of 9.1% of coating, which leads to the diffusion and propagation of corrosion solution and might result in pitting or delamination [42].

The evolution of OCP values before, during, and after tribocorrosion tests in 3.5 wt% NaCl solution are given in Figure 9a. Before the experiment, samples were soaked in 3.5 wt% NaCl solution for 1 h to reach a stable OCP. The tribocorrosion test consists of three regions. In the soaking region (before 10 min), OCP of all samples reached a stable value, and because of the pre-soaking, there was no contact between the counterpart ball and the sample at this stage. Sliding begins at 10 min (sliding process), and the OCP fell rapidly, implying the breaking or removal of the passive film on the surfaces of coatings [43]. Then, when the sliding stops at 40 min, the OCP increases because of the reformation of the passive film. As seen, steel substrate exhibits a large decrease in OCP values when the sliding begins and a low, stable OCP value of −0.41 V in the sliding process. For the Ti-DLC coating deposition at different bias voltages, the coating at −200 V shows the highest stable OCP value of −0.08 V. The OCP value has no significant difference between samples at −50 V and −300 V in the sliding process, which is low and around −0.13 V. The wear rate and coefficient of friction (COF) during sliding for substrate and coatings prepared at different bias voltages are presented in Figure 9b. As seen, the substrate shows a high wear rate of 1.85×10^{-5} $mm^3/N{\cdot}m$ and COF, which is much larger than the values of the coating sample. Combined with OCP results, the substrate shows poor anti-tribocorrosion performance, and the Ti-DLC coating on the steel can dramatically enhance anti-tribocorrosion performance of the substrate. In addition, the OCP of Ti-DLC coatings is consistently lower than the values of the steel substrate, suggesting that the coating has not failed, and the coating provides constant protection to the steel base material during tribocorrosion. With the increase in bias voltage, the COF and wear rate of Ti-DLC coatings both show a trend of increasing firstly and then decreasing. The wear rate of coating prepared at the bias voltages of −50, −100, and −300 V are around 4.01×10^{-7}, 3.32×10^{-7}, and 3.21×10^{-7} $mm^3/N{\cdot}m$, respectively. By contrast, at −200 V, the coatings show the lowest wear rate and COF of 2.48×10^{-7} $mm^3/N{\cdot}m$ and 0.045. Compared with the reported anti-tribocorrosion coatings, the Ti-DLC coatings present lower COF, wear rate, and higher OCP in artificial seawater, indicating that the Ti-DLC coating is a promising candidate material to improve anti-corrosion and -wear properties in the marine environment.

The worn surface and corresponding EDS are given in Figure 10. As shown, the width of wear track of coating at −50 V is 195 μm, and obvious desquamation is observed on the wear scar, which is caused by the interaction of corrosion and wear. The EDS results (Figure 10b) show that the components of coating on the wear track not only contain Ti, C, O, Si, and N, which belong to coating and counterpart, but also contain Na and Cl, which come from artificial seawater solution. The EDS results of coating at different bias voltages are similar. With the increase in bias voltage, the width of wear track is decreased, and some furrows are observed on the wear scar of the coating at −100 V. The coating at −300 V also shows desquamation on the wear track (Figure 10g), suggesting corrosion solution likely penetrating into the coating and reaching the substrate. Corrosion solution

penetrates the coating through the pores, then, under the combined action of friction and corrosion, desquamation and furrows are formed on the worn surface, which could accelerate corrosion and wear and might result in peeling off of the coatings. The generation of desquamation could mainly be responsible for the low OCP value of those coatings.

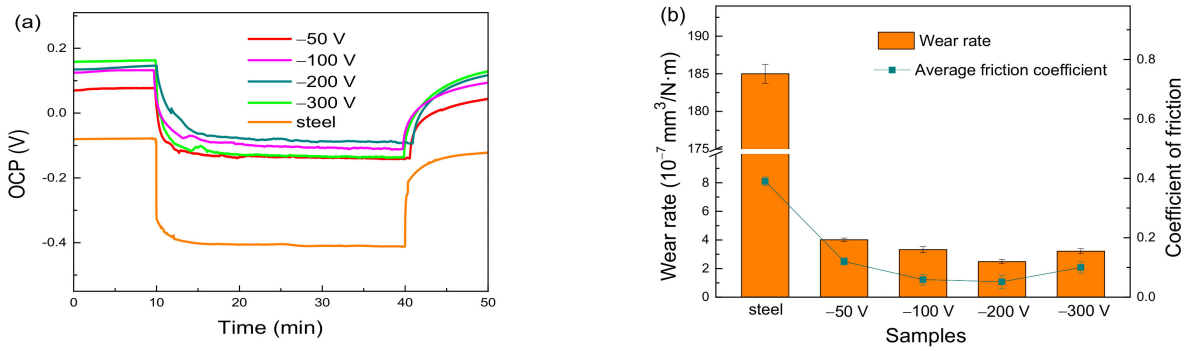

Figure 9. Evolution of OCP values before, during, and after tribocorrosion tests (**a**), and wear rate and friction coefficient during sliding (**b**) for substrate and coatings.

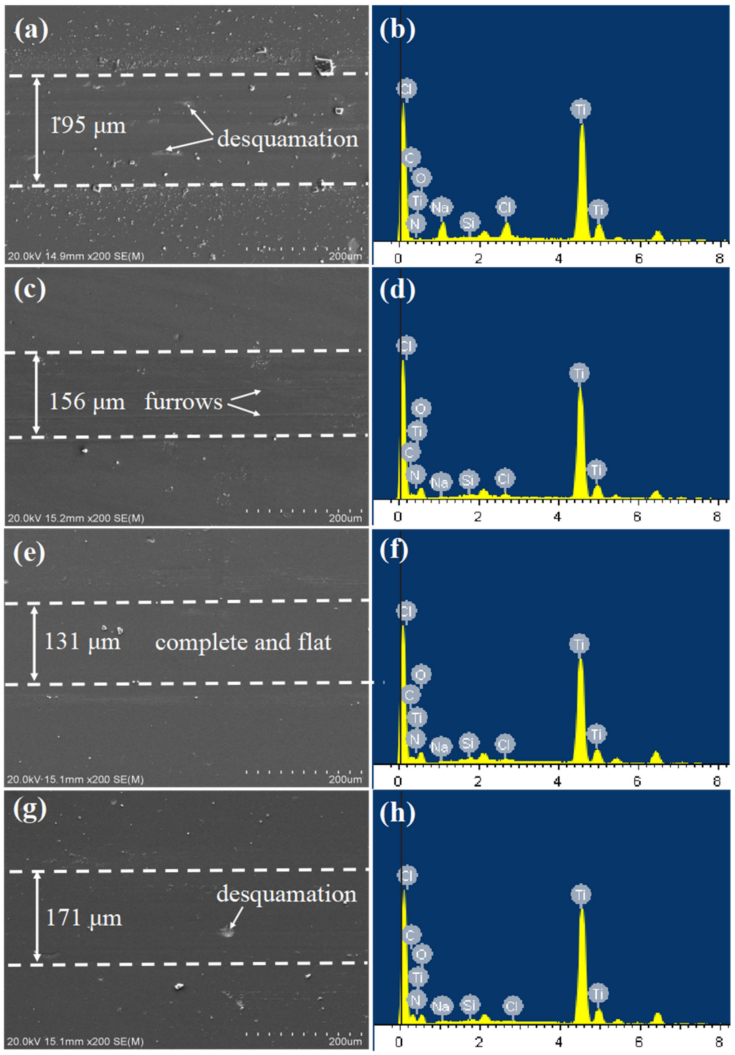

Figure 10. Worn surface and corresponding EDS result of coatings at different bias voltages: (**a**,**b**) −50 V; (**c**,**d**) −100 V; (**e**,**f**) −200 V; (**g**,**h**) −300 V.

According to the results of potentiodynamic polarization curves, the coating at −50 V has high porosity compared to the coating prepared at −100 V and −200 V. Manhabosco and other researchers [41] found that porosity has a huge influence on electrochemical performance of the coating, which could promote the diffusion of water and erosive ions penetrating into the coating, resulting in localized delamination of the coating. During the tribocorrosion test, simultaneous action of friction and corrosion aggravate failure of the coatings, and the diffusion channels of the corrosive medium would be supplied by the micro-cracks, furrows, and desquamation caused by friction force, which leads to the degradation of the coatings [44]. The high porosity of 0.091 of coatings prepared at −50 V would promote the penetration of the erosive ions, which could weaken the adhesion of the coating and substrate, then, under the action of mechanical wear, thus desquamation is observed on the wear scar (Figure 10a). Thereby, the coating at −50 V shows the lowest OCP during the tribocorrosion test. The results of coating at −300 V are similar to the coating prepared at −50 V.

For the coating at −200 V, as seen in Figure 10e, the width of the wear scar is the narrowest (131 μm). In addition, the wear track is flat and smooth, no furrows or desquamation appear on the wear scar, and only small wear debris are observed on the both sides of the worn surface. The samples at −200 V with the narrowest width of the wear track and high OCP value during tribocorrosion test present great anti-tribocorrosion performance under the synergistic action of corrosion and wear, which is mainly due to the dense structure, high value of H/E^* and H^3/E^{*2}, and great corrosion resistance.

4. Conclusions

In this study, Ti-DLC coatings were prepared using the FCVA method by varying bias voltage. The structure and mechanical properties of coatings were investigated, and the corrosion and tribocorrosion performance of coatings under simulated seawater were estimated. As the bias voltage increases, the carbon content increases from 69.3 to 71.3 at.%. The coating showed a typical nanocomposite structure, containing TiC and amorphous carbon phase, which was verified by the results of XPS, XRD, and TEM. With the increase in bias voltage, the grain size of the Ti-DLC coatings was almost consistent. As the bias voltage increased to −200 V, the hardness, corrosion resistance, and anti-tribocorrosion improved, and a further increase in the bias voltage induced a decrease in both the mechanical and tribocorrosion resistance properties. The coating at −200 V with high hardness, H/E^*, dense structure, and good anti-corrosion ability had the minimum COF of 0.052, and the lowest wear rate of 2.48 × $\times 10^{-7}$ $mm^3/N{\cdot}m$, which presents the best tribocorrosion resistance in the artificial seawater environment, implying that Ti-DLC coating shows to be a promising candidate as marine protective material.

Author Contributions: Conceptualization, Y.S. and J.L.; methodology, Y.S. and B.L.; software, Y.S. and Y.Z.; validation, Y.S., L.C. and P.P.; formal analysis, Y.S.; investigation, Y.S., L.C. and P.P.; resources, Y.S. and X.Z. (Xinmiao Zeng); data curation, Y.S.; writing—original draft preparation, Y.S.; writing—review and editing, Y.S., and X.Z. (Xu Zhang); visualization, Y.S. and B.L.; supervision, J.L and X.Z. (Xinmiao Zeng); project administration, Y.S. and J.L.; funding acquisition, Y.S., X.Z. (Xu Zhang) and L.C. All authors have read and agreed to the published version of the manuscript.

Funding: The authors are thankful for the financial support of the China Postdoctoral Science Foundation under Grant No. 2021M690451, National Natural Science Foundation of China under Grant No. 12175019, Youth Program of National Natural Science Foundation of China under Grant No. 12005018.

Institutional Review Board Statement: Not applicable.

Informed Consent Statement: Not applicable.

Data Availability Statement: Data sharing is not applicable to this article.

Conflicts of Interest: The authors declare no conflict of interest.

References

1. Dalmau, A.; Richard, C.; Igual-Muñoz, A. Degradation mechanisms in martensitic stainless steels: Wear, corrosion and tribocorrosion appraisal. *Tribol. Int.* **2018**, *121*, 167–179. [CrossRef]
2. Stachowiak, A.; Zwierzycki, W. Tribocorrosion modeling of stainless steel in a sliding pair of pin-on-plate type. *Tribol. Int.* **2011**, *44*, 1216–1224. [CrossRef]
3. Zhang, Y.; Yin, X.; Wang, J.; Yan, F. Influence of microstructure evolution on tribocorrosion of 304SS in artificial seawater. *Corros. Sci.* **2014**, *88*, 423–433. [CrossRef]
4. Liu, Z.X.; Li, Y.; Xie, X.H.; Qin, J.; Wang, Y. The tribo-corrosion behavior of monolayer VN and multilayer VN/C hard coatings under simulated seawater. *Ceram. Int.* **2021**, *47*, 25655–25663. [CrossRef]
5. Ma, F.; Li, J.; Zeng, Z.; Gao, Y. Structural, mechanical and tribo-corrosion behaviour in artificial seawater of CrN/AlN nano-multilayer coatings on F690 steel substrates. *Appl. Surf. Sci.* **2018**, *428*, 404–414. [CrossRef]
6. Shao, T.; Ge, F.; Dong, Y.; Li, K.; Li, P.; Sun, D.; Huang, F. Microstructural effect on the tribo-corrosion behaviors of magnetron sputtered CrSiN coatings. *Wear* **2018**, *416–417*, 44–53. [CrossRef]
7. Liu, Z.; Ye, Y.; Jiang, Z.; Chen, H.; Song, W.; Liu, Z.; Jia, Y.; Zhu, J. Achieving high anti-wear ability of V–C–N coatings in seawater by carbon content design. *Ceram. Int.* **2020**, *46*, 6612–6620. [CrossRef]
8. Viswanathan, S.; Mohan, L.; Parthasarathi, B.; Shanthiswaroop, S.; Muniprakash, M.; Barshilia, H.C.; Anandan, C. Corrosion and wear resistance properties of multilayered diamond-like carbon nanocomposite coating. *Surf. Interface Anal.* **2018**, *50*, 265–276. [CrossRef]
9. Tyagi, A.; Walia, R.S.; Murtaza, Q.; Pandey, S.M.; Tyagi, P.K.; Bajaj, B. A critical review of diamond like carbon coating for wear resistance applications. *Int. J. Refract. Met. Hard Mater.* **2019**, *78*, 107–122. [CrossRef]
10. Vetter, J. 60 years of DLC coatings: Historical highlights and technical review of cathodic arc processes to synthesize various DLC types, and their evolution for industrial applications. *Surf. Coat. Technol.* **2014**, *257*, 213–240. [CrossRef]
11. Gawel, R.; Kyziol, K.; Jurasz, Z.; Grzesik, Z. Oxidation resistance of valve steels covered with thin SiC coatings, obtained by RF CVD. *Corros. Sci.* **2018**, *145*, 16–25. [CrossRef]
12. Zhang, J.; Wang, Y.; Zhou, S.; Wang, Y.; Wang, C.; Guo, W.; Lu, X.; Wang, L. Tailoring self-lubricating, wear-resistance, anticorrosion and antifouling properties of Ti/(Cu, MoS2)-DLC coating in marine environment by controlling the content of Cu dopant. *Tribol. Int.* **2020**, *143*, 106029. [CrossRef]
13. Cao, H.S.; Ye, X.; Qi, F.G.; Ouyang, X.P.; Zhao, N.; Liao, B. Microstructure, mechanical and tribological properties of multilayer Ti-DLC thick films on Al alloys by filtered cathodic vacuum arc technology. *Mater. Des.* **2021**, *198*, 109320. [CrossRef]
14. Zhang, S.D.; Yan, M.F.; Yang, Y.; Zhang, Y.X.; Yan, F.; Li, H. Excellent mechanical, tribological and anti-corrosive performance of novel Ti-DLC nanocomposite thin films prepared via magnetron sputtering method. *Carbon* **2019**, *151*, 136–147. [CrossRef]
15. Shen, Y.Q.; Luo, J.; Liao, B.; Zhang, X.; Zhao, Y.; Zeng, X.; Chen, L.; Pang, P.; Bao, F. Tribocorrosion and tribological behavior of Ti-DLC coatings deposited by filtered cathodic vacuum arc. *Diam. Relat. Mater.* **2022**, *125*, 108985. [CrossRef]
16. Zhang, K.; Wen, M.; Meng, Q.N.; Hu, C.Q.; Li, X.; Liu, C.; Zheng, W.T. Effects of substrate bias voltage on the microstructure, mechanical properties and tribological behavior of reactive sputtered niobium carbide films. *Surf. Coat. Tech.* **2012**, *212*, 185–191. [CrossRef]
17. Zhang, L.; Ma, G.J.; Ma, H.; Lin, G.Q. Effect of pulsed bias voltage on the structure and mechanical properties of Ti–C–N composite films by pulsed bias arc ion plating. *Nucl. Instrum. Meth. B* **2014**, *333*, 1–5. [CrossRef]
18. Yate, L.; Martínez-de-Olcoz, L.; Esteve, J.; Lousa, A. Effect of the bias voltage on the structure of nc-CrC/a-C: H coatings with high carbon content. *Surf. Coat. Tech.* **2012**, *206*, 2877–2883. [CrossRef]
19. Dai, W.; Zheng, H.; Wu, G.S.; Wang, A.Y. Effect of bias voltage on growth property of Cr-DLC film prepared by linear ion beam deposition technique. *Vacuum* **2010**, *85*, 231–235. [CrossRef]
20. Khamseh, S.; Alibakhshi, E.; Ramezanzadeh, B.; Sari, M. A tailored pulsed substrate bias voltage deposited (a-C: Nb) thin-film coating on GTD-450 stainless steel: Enhancing mechanical and corrosion protection characteristics. *Chem. Eng. J.* **2021**, *404*, 126490. [CrossRef]
21. Sheeja, D.; Tay, B.K.; Yu, L.J.; Lau, S.P.; Sze, J.Y.; Cheong, C.K. Effect of frequency and pulse width on the properties of ta: C films prepared by FCVA together with substrate pulse biasing. *Thin Solid Film.* **2002**, *420*, 62–69. [CrossRef]
22. Shen, Y.Q.; Zhou, H.; Wang, H.Q.; Liao, B.; Zhang, X. Tribological behavior of diamond-like carbon coatings with patterned structure deposited by the filtered cathodic vacuum arc. *Thin Solid Film.* **2019**, *685*, 123–130. [CrossRef]
23. Peng, X.L.; Barber, Z.H.; Clyne, T.W. Surface roughness of diamond-like carbon films prepared using various techniques. *Surf. Coat. Technol.* **2001**, *138*, 23. [CrossRef]
24. Pelleg, J.; Zevin, L.Z.; Lungo, S.; Croitoru, N. Reactive-sputter-deposited TiN films on glass substrates. *Thin Solid Film.* **1991**, *197*, 117–128. [CrossRef]
25. Barna, P.; Adamik, M.; Labar, J.; Kover, L.; Toth, J.; Devenyi, A.; Manaila, R. Formation of polycrystalline and microcrystalline composite thin films by codeposition and surface chemical reaction. *Surf. Coat. Technol.* **2000**, *125*, 147–150. [CrossRef]
26. Alawajji, R.A.; Kannarpady, G.K.; Nima, Z.A.; Kelly, N.; Watanabe, F.; Biris, A.S. Electrical properties of multilayer (DLC-TiC) films produced by pulsed laser deposition. *Appl. Surf. Sci.* **2018**, *437*, 429–440. [CrossRef]
27. Cui, J.; Qiang, L.; Zhang, B.; Ling, X.; Yang, T.; Zhang, J. Mechanical and tribological properties of Ti-DLC films with different Ti content by magnetron sputtering technique. *Appl. Surf. Sci.* **2012**, *258*, 5025–5530. [CrossRef]

28. Zhao, S.S.; Gao, X.H.; Qiu, X.L.; Yu, D.M.; Tian, G.K. A novel TiC-TiN based spectrally selective absorbing coating: Structure, optical properties and thermal stability. *Infrared Phys. Technol.* **2020**, *110*, 1350–4495. [CrossRef]
29. Viswanathan, S.; Reddy, M.M.; Mohan, L.; Bera, P.; Barshilia, H.C.; Anandan, C. Corrosion and Wear Properties of Ti/Tetrahedral Amorphous Carbon Multilayered Coating. *J. Bio. Tribo. Corros.* **2017**, *3*, 39. [CrossRef]
30. Dang, C.; Li, J.; Wang, Y.; Chen, J. Structure, mechanical and tribological properties of self-toughening TiSiN/Ag multilayer coatings on Ti6Al4V prepared by arc ion plating. *Appl. Surf. Sci.* **2016**, *386*, 224–233. [CrossRef]
31. Leyland, A.; Matthews, A. On the significance of the H/E ratio in wear control: A nanocomposite coating approach to optimised tribological behavior. *Wear* **2000**, *246*, 1–11. [CrossRef]
32. Ye, Y.W.; Jiang, Z.L.; Zou, Y.J.; Guo, S.D.; Zeng, X.; Yi, Z.; Yu, J.; Gui, J.; Liu, T.; Chen, H. Enhanced anti-wear property of VCN coating in seawater with the optimization of bias voltage. *Ceram. Int.* **2020**, *46*, 7939–7946. [CrossRef]
33. Hu, J.J.; Zhang, J.Y.; Jiang, Z.H.; Ding, X.; Zhang, Y.; Han, S.; Sun, J.; Lian, J. Plastic deformation behavior during unloading in compressive cyclic test of nanocrystalline copper. *Mater. Sci. Eng. A* **2016**, *651*, 999–1009. [CrossRef]
34. Wang, Y.X.; Wang, L.P.; Zhang, G.G.; Wang, S.C.; Wood, R.J.K.; Xue, Q.J. Effect of bias voltage on microstructure and properties of Ti-doped graphite-like carbon films synthesized by magnetron sputtering. *Surf. Coat. Technol.* **2010**, *205*, 793–800. [CrossRef]
35. Wang, Q.M.; Kim, K.H. Microstructural control of Cr–Si–N films by a hybrid arc ion plating and magnetron sputtering process. *Acta Mater.* **2009**, *57*, 4974–4987. [CrossRef]
36. Guo, J.; Liu, Z.J.; Wang, S.W.; Shen, Y.G. The grain refining effect of energy competition and the amorphous phase in nanocomposite materials. *Scr. Mater.* **2013**, *69*, 662–665. [CrossRef]
37. Díaz, B.; Härkönen, E.; Światowska, J.; Maurice, V.; Seyeux, A.; Marcus, P.; Ritala, M. Low-temperature atomic layer deposition of Al2O3 thin coatings for corrosion protection of steel: Surface and electrochemical analysis. *Corros. Sci.* **2011**, *53*, 2168–2175. [CrossRef]
38. Matthes, B.; Broszeit, E.; Aromaa, J.; Ronkainen, H.; Hannula, S.-P.; Leyland, A.; Matthews, A. Corrosion performance of some titanium-based hard coatings. *Surf. Coat. Technol.* **1991**, *49*, 489–495. [CrossRef]
39. Ye, Y.; Liu, Z.; Liu, W.; Zhang, D.; Zhao, H.; Wang, L.; Li, X. Superhydrophobic oligoaniline-containing electroactive silica coating as pre-process coating for corrosion protection of carbon steel. *Chem. Eng. J.* **2018**, *348*, 940–951. [CrossRef]
40. Ye, Y.; Zhang, D.; Liu, T.; Liu, Z.; Liu, W.; Pu, J.; Chen, H.; Zhao, H.; Li, X. Improvement of anticorrosion ability of epoxy matrix in simulate marine environment by filled with superhydrophobic POSS-GO nanosheets. *J. Hazard. Mater.* **2019**, *364*, 244–255. [CrossRef]
41. Manhabosco, T.M.; Müller, I.L. Tribocorrosion of Diamond-Like Carbon Deposited on Ti6Al4V. *Tribol. Lett.* **2009**, *33*, 193–197. [CrossRef]
42. Hübler, R.; Schröer, A.; Ensinger, W.; Wolf, G.K.; Schreiner, W.H.; Baumvol, I.J.R. Plasma and ion-beam-assisted deposition of multilayers for tribological and corrosion protection. *Surf. Coat. Technol.* **1993**, *60*, 561–565. [CrossRef]
43. Wang, Y.; Li, J.L.; Dang, C.Q.; Wang, Y.X.; Zhu, Y. Influence of carbon contents on the structure and tribocorrosion properties of TiSiCN coatings on Ti6Al4V. *Tribol. Int.* **2017**, *109*, 285–296. [CrossRef]
44. Warcholinski, B.; Gilewicz, A. Multilayer coatings on tools for woodworking. *Wear* **2011**, *271*, 2812–2820. [CrossRef]